ACS ES&T Engineering

pubs.acs.org/estengg

Article

Modulating the Dispersion of Ce on CeO_2/TiO_2 Catalysts for Efficient NH_3−SCR of NO

Published as part of ACS ES&T Engineering special issue "Environmental Catalysis for Air Pollution Control".

Nan Jiang,[⊥] Jiawei Yang,[⊥] Yirui Yang, Wu Gao, Kaili Ma, Xiuwen Wang, Qiuhui Qian, Qing Tong,* Wei Tan,* and Lin Dong*

Cite This: ACS EST Engg. 2025, 5, 2060−2069

Read Online

ACCESS | Metrics & More | Article Recommendations | Supporting Information

ABSTRACT: CeO_2−TiO_2 catalysts have been intensively investigated for their promising application prospect in the selective catalytic reduction of NO by NH_3 (NH_3−SCR of NO). However, the optimal dispersion of CeO_2 on CeO_2−TiO_2 catalysts is still controversial. In this work, using $TiO(OH)_2$ and TiO_2 as supports and different Ce precursors, TiO_2-supported CeO_2 with a controllable dispersion was prepared. It was uncovered that hydroxyl groups on $TiO(OH)_2$ could facilitate the even dispersion of Ce (high dispersion, Ce/Ti−H), while the impregnation of cerium oxalate onto TiO_2 would result in the generation of highly crystalline CeO_2 (low dispersion, Ce/Ti-L), even with a low CeO_2 loading of 5 wt %. When cerium nitrates were impregnated onto TiO_2, slightly crystalline CeO_2 (moderate dispersion, Ce/Ti-M) was successfully fabricated. The NH_3−SCR activity on the prepared CeO_2/TiO_2 catalysts followed an order of Ce/Ti-M > Ce/Ti−H > Ce/Ti-L, suggesting that small CeO_2 particles on TiO_2 could better facilitate the proceeding of the NH_3−SCR reaction. According to the results of the mechanism study, the superior redox capability of Ce/Ti-M enabled efficient activation of reactants, thus achieving the best NH_3−SCR activity. This study provided a strategic framework for the design of high-performance catalysts by precisely engineering the dispersion of active species at the nanoscale.

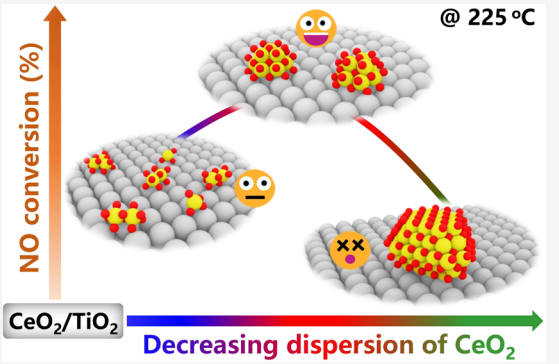

KEYWORDS: *dispersion of CeO_2, CeO_2−TiO_2 catalysts, surface hydroxyl groups, redox performance, reactant activation*

1. INTRODUCTION

Nitrogen oxides (NO_x), as one of the typical air pollutants, could pose a severe threat to human health and the ecological environment.[1] In the field of NO_x emission control, selective catalytic reduction of NO_x with NH_3 (NH_3−SCR) technology has received great attention due to its high efficiency.[2,3] With the increasingly stringent emission control regulations, the development of adapted catalysts with better catalytic performance has long been a research hotspot.[4,5]

TiO_2 materials have been widely applied in the construction of NH_3−SCR catalysts for decades, which not only offered high specific surface area and good thermal stability but also provided abundant acid sites, thus improving the catalytic performance of the catalysts.[6−8] In general, V_2O_5/TiO_2 and its derived catalysts were the most successful catalysts for the NH_3−SCR of NO_x. Previously, it has been reported that the dispersion of V species on the TiO_2 support played a key role in determining the catalytic performance of V_2O_5/TiO_2 catalysts.[9−13] For example, by tuning the dynamic evolution of vanadium oxide species on TiO_2, Lian et al. revealed that polymeric vanadyl species exhibited markedly higher activity than monomeric vanadyl species and crystalline V_2O_5 species in the NH_3−SCR reaction.[10−12] However, the relatively inferior low-temperature NH_3−SCR activity, low N_2 selectivity, potential N_2O emission risk, and the biotoxicity of vanadium still hindered the further use of V_2O_5/TiO_2 catalysts in future industrial applications.[14,15]

Recently, TiO_2-supported CeO_2 or CeO_2−TiO_2 mixed oxide catalysts have been recognized as promising candidates for efficient NH_3−SCR of NO_x due to their excellent NH_3−SCR activity and significant advantages in terms of environmental friendliness.[16,17] Typically, due to the overlap of energy levels in the Ce 4f-5d orbitals, as depicted in the Cotton atomic orbital energy level diagram, the redox pair of $Ce^{3+} \leftrightarrow Ce^{4+}$ (electron gain or loss) within CeO_2 can effectively promote the activation of O_2 through the oxygen storage−release cycle,[18] which in turn activated NH_3 and NO molecules, and thus

Received: February 18, 2025
Revised: April 15, 2025
Accepted: April 15, 2025
Published: April 23, 2025

https://doi.org/10.1021/acsestengg.5c00151
ACS EST Engg. 2025, 5, 2060−2069

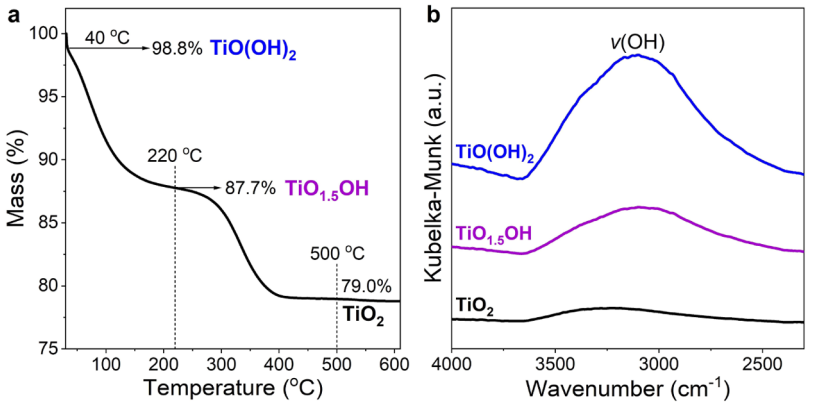

Figure 1. (a) TG profiles for $TiO(OH)_2$. (b) ATR-FTIR spectra for $TiO(OH)_2$, $TiO_{1.5}OH$, and TiO_2.

generating superior low-temperature NH_3−SCR activity.[19] In addition, the Ce−Ti interaction as well as the acid sites provided by TiO_2 could further contribute to the proceeding of the NH_3−SCR reaction. To further tap the potential of CeO_2−TiO_2 catalysts, various strategies, including morphology/crystal phase control,[20] Ce−Ti interface engineering,[21] surface modification,[22] etc., have been applied. For example, CeO_2 supported on a TiO_2 nanotube showed higher dispersion and exhibited better NH_3−SCR activity.[23] Moreover, hollow-structured CeO_2−TiO_2 catalysts with large cavities exhibited superior SO_2 resistance in the NH_3−SCR reaction.[24] Previously, we also reported that CeO_2 coated with a TiO_2 layer exhibited satisfactory NH_3−SCR activity and SO_2 resistance.[21] In addition, surface acidity modification was also proved to be effective in improving the catalytic performance of CeO_2−TiO_2 catalysts.[25] As discussed above, a series of highly efficient CeO_2−TiO_2 catalysts have been developed; however, the optimal dispersion of CeO_2 on TiO_2 in the NH_3−SCR reaction has not been clarified yet. In particular, amorphous CeO_2 (or amorphous $CeTiO_x$) and slightly crystalline CeO_2 were recognized as the most active species in different studies.[26−28] Notably, to the best of our knowledge, there is still no facile preparation method for the construction of CeO_2 with controllable dispersion on a TiO_2 support, hampering researchers from determining the optimal dispersion of CeO_2.

In this work, building upon our previous findings that the hydroxyl groups on supports as well as the precursors of active species showed a significant impact on the dispersion of active species,[29,30] a simple but effective strategy was proposed to fine-tune the dispersion of CeO_2 on the TiO_2 support, and serial CeO_2/TiO_2 catalysts with distinct CeO_2 dispersion were fabricated. According to the results of catalytic performance evaluation and detailed characterizations, it was disclosed that slightly crystalline CeO_2 on TiO_2 exhibited a much better NH_3−SCR activity than amorphous CeO_2 and highly crystalline CeO_2 due to its superior low-temperature redox capability. This work would benefit the future design of robust CeO_2−TiO_2 catalysts for the NH_3−SCR of NO.

2. METHODS

2.1. Catalyst Preparation. $TiO(OH)_2$ and TiO_2 supports were prepared by a modified sol−gel method. Specifically, 20 mL of tetrabutyl titanate (TBOT) and 20 mL of ethanol were first mixed and stirred to form a uniform solution, and then a mixture of 20 mL of ethanol, 10 mL of acetic acid, and 10 mL of deionized water was added to the above solution under vigorous stirring. The obtained system was aged at room temperature for 48 h, followed by being dried in an oil bath at 60 °C for 8 h. The resulting gel was washed with ethanol and deionized water several times to remove impurities and subsequently dried in an oven at 40 °C for 12 h. The obtained solid was ground and ready for use, denoted as $TiO(OH)_2$. TiO_2 was prepared by calcined $TiO(OH)_2$ at 500 °C for 4 h.

To realize the modulation of Ce dispersion on TiO_2, different supports ($TiO(OH)_2$ and TiO_2) and Ce precursors ($Ce(NO_3)_3{\cdot}6H_2O$ and $Ce_2(C_2O_4)_3{\cdot}10H_2O$) were used. A traditional incipient wetness impregnation (IWI) method was used to deposit CeO_2 onto TiO_2. The loading amount of CeO_2 was controlled at 5 wt %. After impregnation, the mixture was calcined at 500 °C for 2 h. CeO_2/TiO_2 prepared with $Ce(NO_3)_3{\cdot}6H_2O$ and $TiO(OH)_2$ was denoted as Ce/Ti−OH-N or Ce/Ti−H (−H = high dispersion). CeO_2/TiO_2 prepared with $Ce(NO_3)_3{\cdot}6H_2O$ and TiO_2 was denoted as Ce/Ti−N or Ce/Ti-M (−M = medium dispersion). CeO_2/TiO_2 prepared with $Ce_2(C_2O_4)_3{\cdot}10H_2O$ and TiO_2 was denoted as Ce/Ti−O or Ce/Ti-L (−L = low dispersion). It should be noted that the impregnation liquid containing $Ce_2(C_2O_4)_3$ was actually a $Ce_2(C_2O_4)_3$ suspension, since $Ce_2(C_2O_4)_3{\cdot}10H_2O$ was almost insoluble in water.[31] For better comprehension, the detailed synthesis procedure is also illustrated in Figure S1.

2.2. Catalyst Characterization. The detailed descriptions of catalyst characterization can be found in the Supporting Information (Text S1).

2.3. Catalytic Performance Evaluation. A fixed-bed quartz tube reactor was used to evaluate the catalytic performance of the prepared catalysts in the NH_3−SCR reaction. In each test, 100 mg of catalyst (40−60 mesh) was loaded into the quartz tube, and the inlet gas with a flow rate of 100 mL·min^{-1} was composed of 500 ppm of NO, 500 ppm of NH_3, 100 ppm of SO_2 (when used), 5% H_2O (when used), and 5% O_2, using N_2 as a balance. The weight hourly space velocity was 60,000 mL·g·h^{-1}. The composition of the outlet gas was analyzed by an online Thermo Nicolet iS10 FTIR spectrometer equipped with a 2 m path-length gas cell. NO conversion and N_2 selectivity on the prepared catalysts in the NH_3−SCR reaction were calculated as follows:

$$\text{NO conversion (\%)} = \frac{[\text{NO}]_{\text{in}} - [\text{NO}]_{\text{out}}}{[\text{NO}]_{\text{in}}} \times 100\%$$

https://doi.org/10.1021/acsestengg.5c00151
ACS EST Engg. 2025, 5, 2060−2069

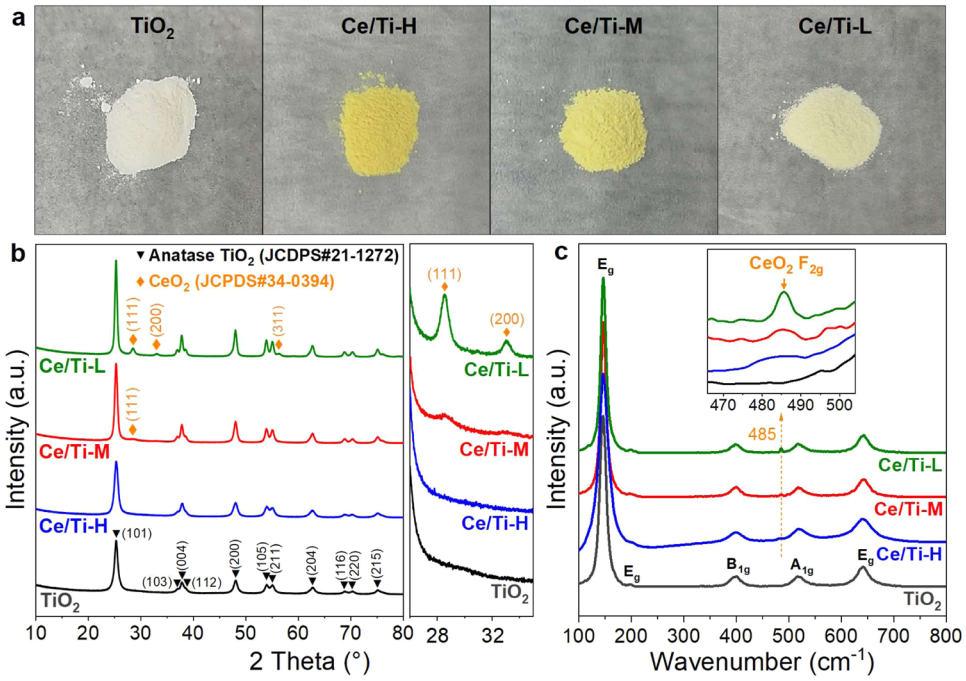

Figure 2. (a) Photographs of the TiO_2 support and CeO_2/TiO_2 catalysts. (b) XRD patterns and (c) Raman spectra for the TiO_2 support and CeO_2/TiO_2 catalysts.

$$N_2\ \text{selectivity}\ (\%) = \frac{[NH_3]_{in}+[NO]_{in}-[NH_3]_{out}-[NO]_{out}-[NO_2]_{out}-2[N_2O]_{out}}{[NH_3]_{in}+[NO]_{in}-[NH_3]_{out}-[NO]_{out}} \times 100\%$$

The method for the catalytic performance evaluation in NH_3 oxidation and NO oxidation reaction can be found in the Supporting Information (Text S2).

3. RESULTS AND DISCUSSION

3.1. Structural Information. The TG experiment was first conducted on $TiO(OH)_2$ to confirm its exact composition. As shown in Figure 1a, three weight loss steps were observed. The first weight loss step (from 100 to 98.8%) at ca. 40 °C was attributed to the desorption of H_2O and impurities adsorbed on the powder. The next two significant weight loss steps (40−220 and 220−500 °C) should be related to the dehydration process of $TiO_x(OH)_y$.[32] Considering that the residual obtained at 500 °C could be approximated as TiO_2, the product after the first weight loss step can be calculated as $TiO_{0.9}(OH)_{2.2}$ based on the weight loss value (from 98.8 to 79%), which was close to that of $TiO(OH)_2$. That is, $TiO(OH)_2$ was successfully prepared in this work. In addition, the product obtained at 220 °C was determined as $TiO_{1.5}OH$.

An ATR-FTIR experiment was carried out to visualize the different concentrations of hydroxyl groups on $TiO(OH)_2$ and TiO_2. As shown in Figure 1b, the broad band within the range of 3000−3500 cm^{-1} observed on $TiO(OH)_2$, $TiO_{1.5}OH$, and TiO_2 was assigned to the hydroxyl species (ν(OH)).[33,34] However, the ν(OH) band on $TiO(OH)_2$ was much more intensive than that on TiO_2, suggesting the existence of abundant hydroxyl groups on $TiO(OH)_2$.

As exhibited in Figure 2a, CeO_2/TiO_2 catalysts prepared with different supports and Ce precursors showed distinct colors, indicating the various dispersion of CeO_2. Hence, XRD patterns for TiO_2 and supported CeO_2 catalysts were collected to determine their crystal phase and the dispersion of CeO_2. As demonstrated in Figure 2b, all XRD peaks on TiO_2 could be indexed to anatase TiO_2 (JCPDS#21-1272). For Ce/Ti−OH-N, no additional XRD peaks attributed to CeO_2 species were detected, indicating that $TiO(OH)_2$ could facilitate the dispersion of CeO_2. For Ce/Ti−N prepared by impregnating $Ce(NO)_3{\cdot}6H_2O$ onto TiO_2, a weak XRD peak located at *ca.* 28.5 ° was observed, which could be attributed to the (111) facet of CeO_2 (JCPDS#34-0394). When changing the Ce precursor from $Ce(NO)_3{\cdot}6H_2O$ to $Ce_2(C_2O_4)_3{\cdot}10H_2O$, the crystallinity of CeO_2 on Ce/Ti−O further increased, suggesting the lower dispersion of CeO_2. That is, the dispersion of Ce on three CeO_2/TiO_2 catalysts followed an order of Ce/Ti−OH-*N* > Ce/Ti-N > Ce/Ti−O. For better understanding, Ce/Ti−OH-N, Ce/Ti−N, and Ce/Ti−O were renamed as Ce/Ti−H, Ce/Ti-M, and Ce/Ti-L, respectively (−H = high dispersion, −M = medium dispersion, −L = low dispersion). In addition, the results of XPS analysis also showed that the highest surface Ce concentration was achieved on Ce/Ti−H (Table S1).

The crystal phase of TiO_2 as well as the dispersion of CeO_2 on CeO_2/TiO_2 catalysts was also evaluated by Raman spectra (Figure 2c). Five peaks at 146, 198, 398, 519, and 642 cm^{-1} observed on the TiO_2 support could be ascribed to Raman active modes of anatase TiO_2 with symmetries of E_g, E_g, B_{1g}, A_{1g}, and E_g, respectively.[35] After the deposition of CeO_2, Raman shift peaks associated with the F_{2g} mode of CeO_2 emerged at 485 cm^{-1},[36] and the intensity of the CeO_2 F_{2g} peak also followed an order of Ce/Ti-L > Ce/Ti-M > Ce/Ti−H, matching well with the results of XRD. According to the results of N_2-physisorption (Table S2 and Figures S2 and S3), although Ce/Ti-H (101.5 $m^2{\cdot}g^{-1}$) showed a higher specific surface area than TiO_2 (77.9 $m^2{\cdot}g^{-1}$), Ce/Ti-M (66.2 $m^2{\cdot}g^{-1}$) and Ce/Ti-L (67.2 $m^2{\cdot}g^{-1}$), which should be due to the formation of the Ce−O−Ti interaction between highly dispersed CeO_2 and TiO_2 on Ce/Ti−H during the calcination

https://doi.org/10.1021/acsestengg.5c00151
ACS EST Engg. 2025, 5, 2060−2069

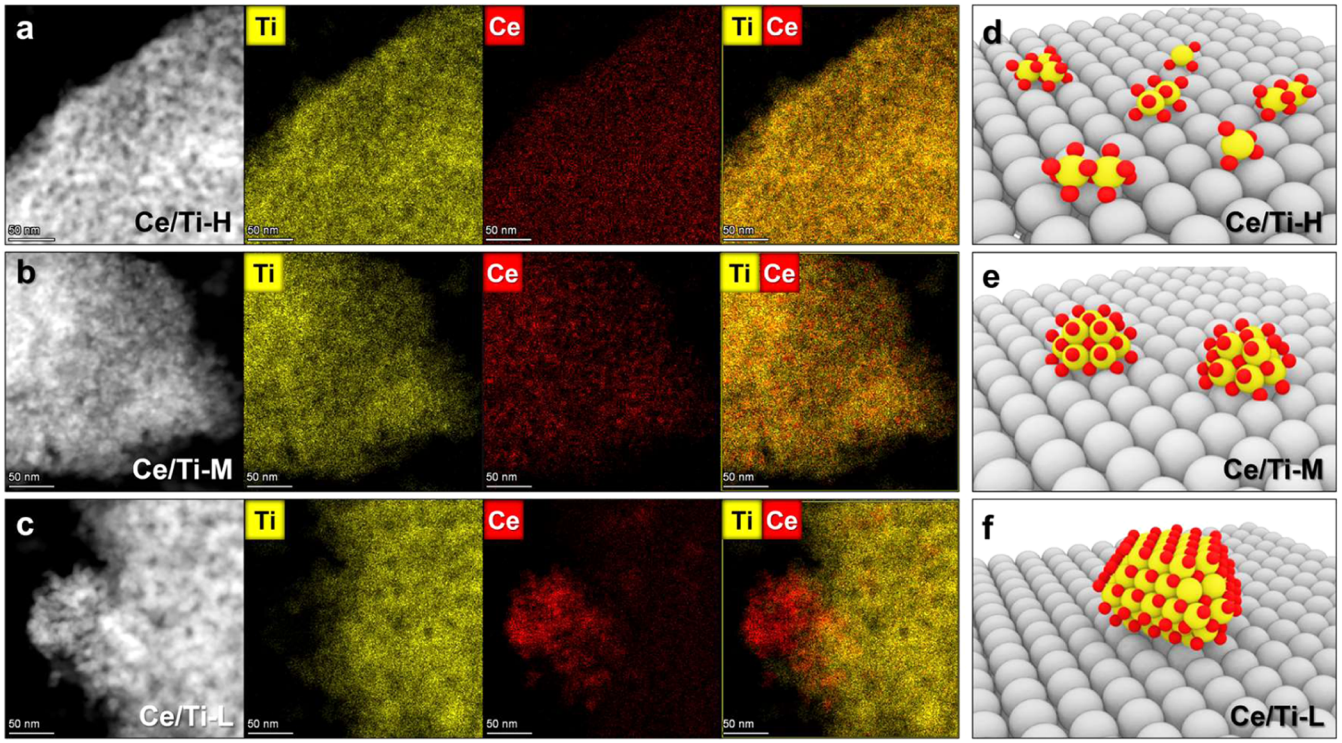

Figure 3. HAADF-STEM images and the corresponding EDS elemental mapping images of (a) Ce/Ti−H, (b) Ce/Ti-M, and (c) Ce/Ti-L. Surface models for (d) Ce/Ti−H, (e) Ce/Ti-M, and (f) Ce/Ti-L.

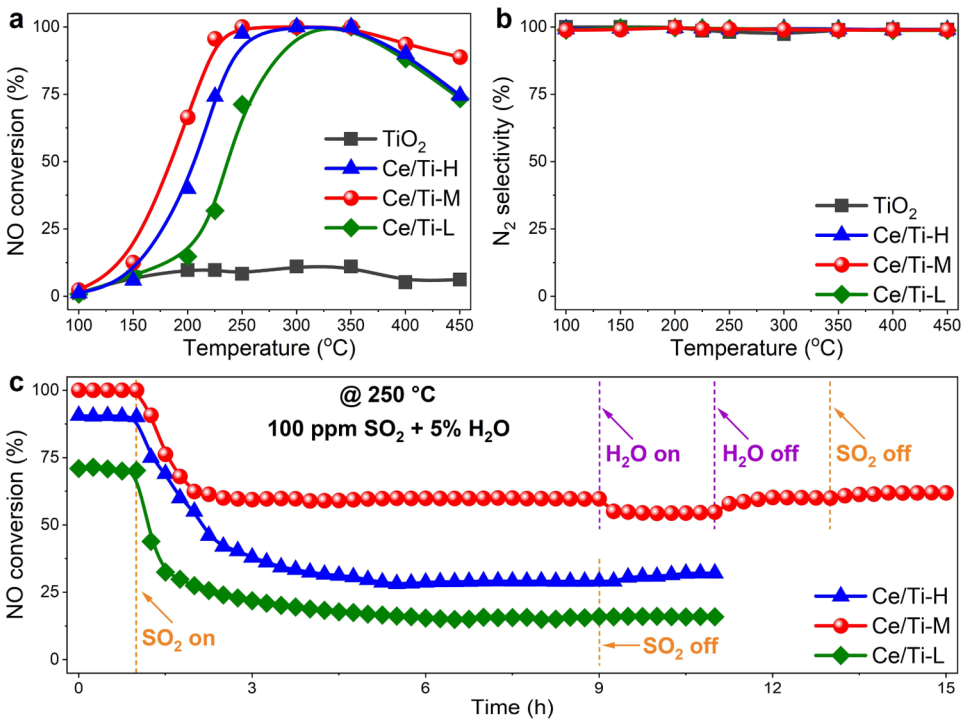

Figure 4. (a) NO conversion and (b) N_2 selectivity on TiO_2 and CeO_2/TiO_2 catalysts in the NH_3−SCR reaction. (c) NO conversion on CeO_2/TiO_2 catalysts in the NH_3−SCR reaction with the addition of SO_2 and H_2O into the feeding gas. Reaction conditions: 500 ppm of NO, 500 ppm of NH_3, 5% O_2, 100 ppm of SO_2 (when used), and 5% H_2O (when used), using Ar as a balance, WHSV = 60,000 mL·g^{-1}·h^{-1}.

process, TiO_2 and CeO_2/TiO_2 catalysts showed similar pore structures.

Since it was difficult to directly recognize CeO_2 on the TiO_2 support by HR-TEM and HAADF-STEM technologies, EDS elemental mapping images were collected to evaluate the size of CeO_2 species on CeO_2/TiO_2 catalysts (Figures S4−S6 and 3). As shown in Figure 3a, even a dispersion of Ce was observed on Ce/Ti−H, indicating the high dispersion of CeO_2. For Ce/Ti-M, a slight agglomeration of CeO_2 was observed (Figure 3b). Moreover, significant aggregation of CeO_2 was

https://doi.org/10.1021/acsestengg.5c00151
ACS EST Engg. 2025, 5, 2060−2069

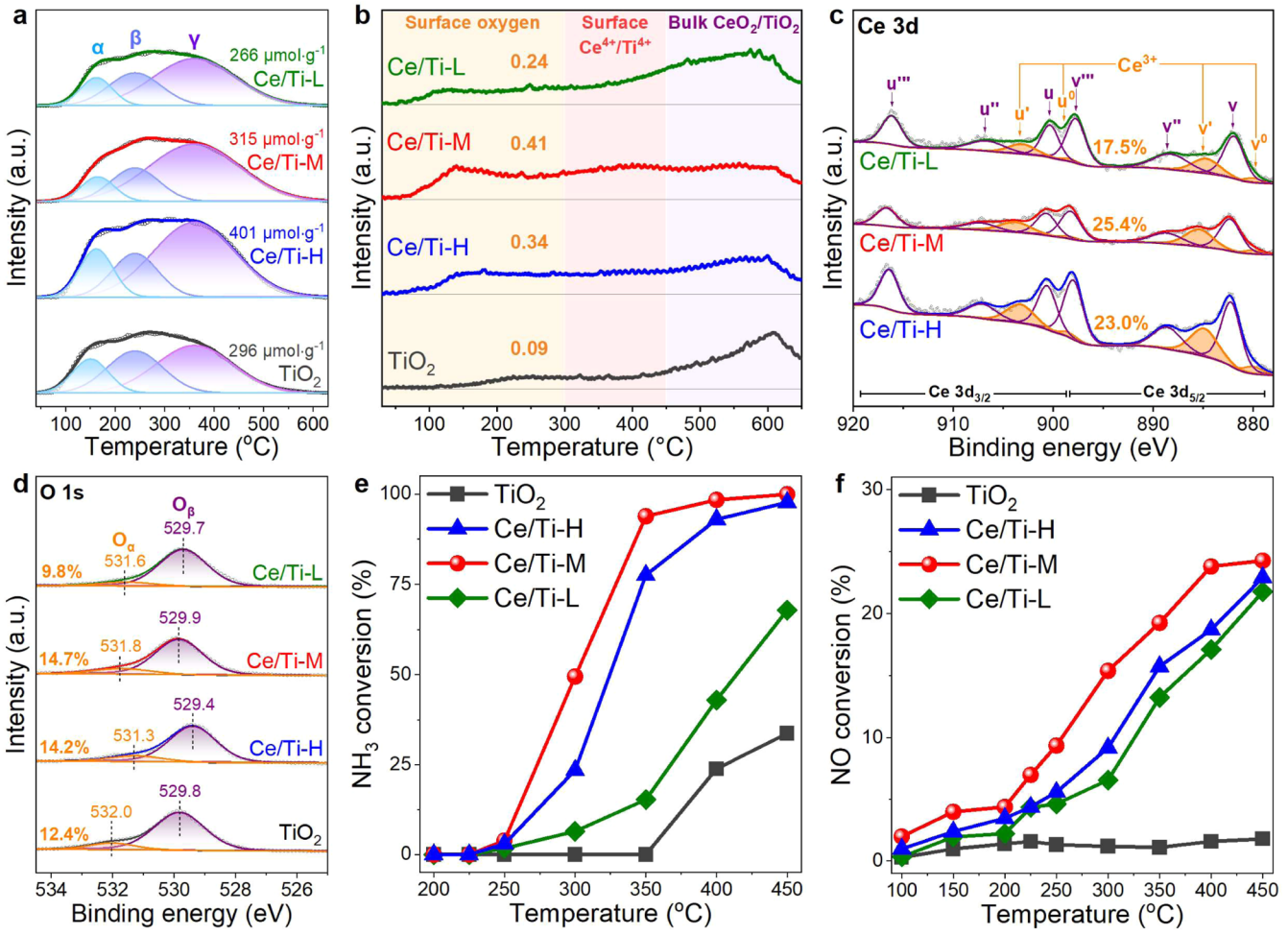

Figure 5. (a) NH_3-TPD profiles and (b) CO-TPR profiles for TiO_2 and CeO_2/TiO_2 catalysts. (c) Ce 3d XPS for CeO_2/TiO_2 catalysts. (d) O 1s XPS for TiO_2 and CeO_2/TiO_2 catalysts. (e) NH_3 conversion on TiO_2 and CeO_2/TiO_2 catalysts in the NH_3 oxidation reaction. (f) NO conversion on TiO_2 and CeO_2/TiO_2 catalysts in the NO oxidation reaction.

found on Ce/Ti-L (Figure 3c). Several crystalline CeO_2 particles were also observed in the HR-TEM images of Ce/Ti-L (Figure S6). The results of EDS elemental mapping matched the conclusion drawn from XRD, XPS, and Raman spectra that the dispersion of CeO_2 on CeO_2/TiO_2 catalysts followed an order of Ce/Ti−H > Ce/Ti-M > Ce/Ti-L (Figure 3d−f). In short summary, due to the unique function of hydroxyl groups on $TiO(OH)_2$ in facilitating the dispersion of CeO_2, as well as the distinct nature of $Ce(NO_3)_3{\cdot}6H_2O$ and $Ce_2(C_2O_4)_3{\cdot}10H_2O$, CeO_2/TiO_2 catalysts with different CeO_2 dispersions were successfully prepared.

3.2. Catalytic Performance in NH_3−SCR Reactions. CeO_2−TiO_2 catalysts have been intensively studied in the NH_3−SCR reaction.[37] However, the optimal dispersion of CeO_2 on CeO_2−TiO_2 catalysts for the NH_3−SCR of NO has not been clarified. In this work, the catalytic performance of TiO_2, Ce/Ti−H, Ce/Ti-M, and Ce/Ti-L in the NH_3−SCR reaction was evaluated.

As illustrated in Figure 4a, after the impregnation of CeO_2, the catalytic performance of TiO_2 was drastically improved, indicating that the synergistic effect between CeO_2 and TiO_2 was the key to high NH_3−SCR activity. Interestingly, the NH_3−SCR activity on CeO_2/TiO_2 catalysts followed a sequence of Ce/Ti-M > Ce/Ti−H > Ce/Ti-L, which implied that TiO_2-supported CeO_2 with a medium dispersion could better catalyze the NH_3−SCR reaction. Moreover, the low T_{90} (the temperature at which the NO conversion reached 90%) of *ca.* 220 °C and the wide operating temperature window (220−400 °C) on Ce/Ti-M made it comparable to those of recently reported novel CeO_2−TiO_2-based catalysts (Table S3). In addition, all CeO_2/TiO_2 catalysts showed high N_2 selectivity (> 95%) throughout the test (Figure 4b).

To further highlight the unique role of hydroxyl groups on $TiO_x(OH)_y$ in tuning the dispersion and catalytic performance of CeO_2, CeO_2 (5 wt %) supported on $TiO_{1.5}OH$ (Ce/$TiO_{1.5}OH$) was also prepared and applied in NH_3−SCR of NO reaction (Figures S7 and S8). It was found that the activity on $CeO_2/TiO_{1.5}OH$ at low temperatures (< 250 °C) was higher than that on Ce/Ti−H but still slightly lower than that on Ce/Ti-M.

In the practical application of NH_3−SCR catalysts, SO_2/H_2O poisoning is an unavoidable obstacle. To evaluate the industrial application prospect of Ce/Ti-M, the catalytic performance of CeO_2/TiO_2 catalysts in the presence of SO_2 and H_2O was tested at 250 °C (Figure 4c). Upon the introduction of SO_2 (100 ppm) to the feeding gas, NO conversion on Ce/Ti−H, Ce/Ti-M, and Ce/Ti-L decreased accordingly, which meant that SO_2 could result in the deactivation of all CeO_2/TiO_2 catalysts. After several hours, the NO conversion on Ce/Ti−H, Ce/Ti-M, and Ce/Ti-L

https://doi.org/10.1021/acsestengg.5c00151
ACS EST Engg. 2025, 5, 2060−2069

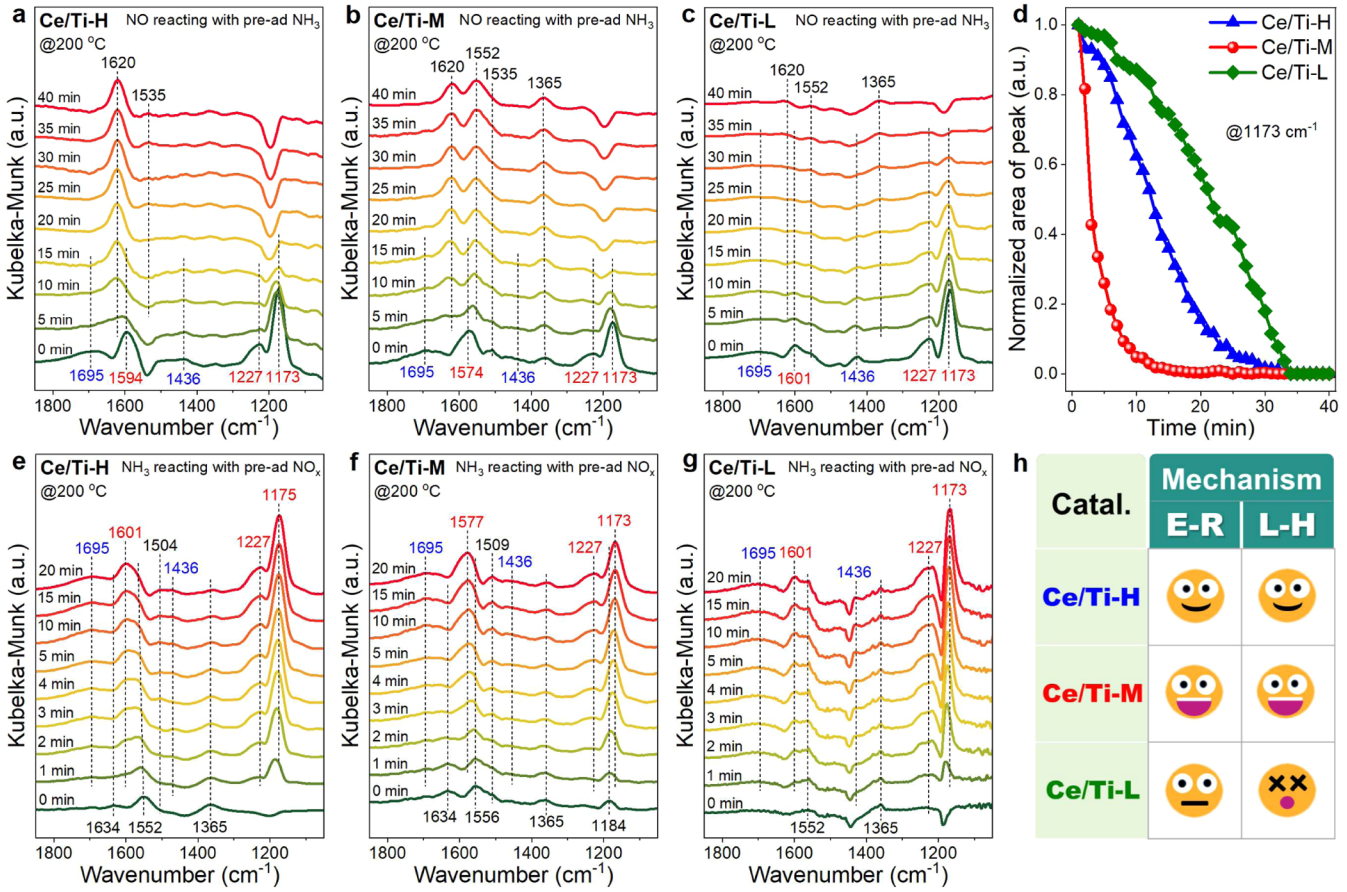

Figure 6. *In situ* DRIFTs of NO + O_2 reacting with preadsorbed NH_3 on (a) Ce/Ti−H, (b) Ce/Ti-M, and (c) Ce/Ti-L at 200 °C. (d) Normalized peak area centered at 1173 cm^{-1} as a function of reaction time. *In situ* DRIFTs of NH_3 reacting with preadsorbed NO_x on (e) Ce/Ti−H, (f) Ce/Ti-M, and (g) Ce/Ti-L at 200 °C. (h) Illustration of dominant reaction pathways on Ce/Ti−H, Ce/Ti-M, and Ce/Ti-L.

stabilized at 29, 60, and 15%, respectively. That is, Ce/Ti-M still substantially outperformed Ce/Ti−H and Ce/Ti-L in the presence of SO_2. Furthermore, when 5% H_2O was also switched on, the NO conversion on Ce/Ti-M only slightly decreased, and then quickly recovered upon switching off H_2O, indicating that the competitive adsorption between H_2O and reactants was the main reason for the deactivation caused by H_2O. However, turning off SO_2 would not result in the obvious increase of NO conversion on Ce/Ti-M, which meant that the deactivation caused by SO_2 was almost irreversible at 250 °C. To reveal the reasons for the deactivation of Ce/Ti-M in the presence of SO_2, temperature-programmed desorption (TPD) experiments were conducted on the spent catalysts (treated with NH_3−SCR + SO_2 reaction flow for 8 h). As shown in Figure S9, the intensity of the SO_2-desorption peak on Ce/Ti-M was more intensive than that on Ce/Ti−H and Ce/Ti-L, suggesting that small CeO_2 particles on Ce/Ti-M showed a stronger affinity for SO_2. Moreover, an *in situ* DRIFTS of NH_3−SCR + SO_2 experiment was performed on Ce/Ti-M at 250 °C to determine the deposited sulfate species (Figure S10). Several IR bands attributed to sulfate species (1250−1350 cm^{-1}) and NH_4^+ species (1436 and 1695 cm^{-1}) emerged after switching on SO_2, which should be related to the formation of ceric sulfates or ammonium sulfates.[38] When using the ATR-FTIR spectra for $(NH_4)_2SO_3$, $(NH_4)_2SO_4$, and NH_4HSO_4 as references, it was found that IR characteristic peaks for them did not match those IR bands attributed to sulfate species on Ce/Ti-M well (Figure S11), suggesting that the intensive IR bands assigned to NH_4^+ were mainly related to the accumulation of ceric sulfates serving as Brønsted acid sites. That is, the main reason for the irreversible deactivation of Ce/Ti-M was the sulfation of the surface metal sites.

3.3. Surface Acidity and Redox Performance. Since the NH_3−SCR reaction was composed of two half reactions, i.e., acid cycle and redox cycle,[39] surface acidity and the redox performance of CeO_2/TiO_2 catalysts were investigated. The NH_3-TPD experiment was first conducted, and the results are shown in Figure 5a and Table S4. It was found that the NH_3 desorption amount on the TiO_2 support and CeO_2/TiO_2 catalysts was roughly positively correlated with the surface area. Ce/Ti−H with the largest specific surface area (101.5 $m^2 \cdot g^{-1}$) showed the highest NH_3 desorption amount (401 μmol of $NH_3 \cdot g^{-1}$). TiO_2, Ce/Ti-M, and Ce/Ti-L with comparable specific surface areas (ca. 70 $m^2 \cdot g^{-1}$) possessed similar NH_3 adsorption amounts (ca. 300 μmol $NH_3 \cdot g^{-1}$). When the results of N_2-physisorption were taken into consideration, it was found that more surface acid sites were formed on Ce/Ti-M per unit surface area (Figure S12a). It was also noted that the ratio of peaks β and γ to the total NH_3-desorption peak area on Ce/Ti-M surpassed that on Ce/Ti-L and Ce/Ti−H (Figure S12b), indicating that Ce/Ti-M showed a higher average acid strength. That is, Ce/Ti-M showed the best surface acidity in terms of acid site amount per unit area and average acid strength, which might also contribute to its better catalytic performance in the NH_3−SCR reaction.

https://doi.org/10.1021/acsestengg.5c00151
ACS EST Engg. 2025, 5, 2060−2069

A CO-TPR experiment was carried out to investigate the redox property of CeO_2/TiO_2 catalysts. As shown in Figure 5b, CO-TPR profiles for all samples could be divided into three regions, which should be related to the reduction of surface oxygen species (< 300 °C), surface Ti^{4+} or Ce^{4+} species (300−450 °C), and bulk TiO_2 or CeO_2 species (> 450 °C). When the CO consumption amount on TiO_2 was normalized to 1.00, the normalized CO consumption amount corresponding to different species on various catalysts was calculated and is listed in Table S5. It was found that the CO consumption amount associated with surface oxygen species on TiO_2 and CeO_2/TiO_2 followed an order of Ce/Ti-M (0.41) > Ce/Ti−H (0.34) > Ce/Ti-L (0.24) > TiO_2 (0.09), which corresponded well to the sequence of their low-temperature NH_3−SCR activity. In addition, the result of CO-TPR also matched well with that of H_2-TPR (Figure S13 and Table S6). That is, the low-temperature redox capability of CeO_2/TiO_2 catalysts played a decisive role in the NH_3−SCR reaction. The significantly different low-temperature redox capability should be directly related to the different dispersions of the loaded CeO_2. CeO_2 with a moderate dispersion showed better redox performance than highly dispersed CeO_2 or highly crystallized CeO_2.

It has been reported that the smaller CeO_2 particle size would facilitate the formation of more Ce^{3+}, surface oxygen defects and adsorbed oxygen species.[40−42] XPS experiments were carried out to characterize the surface chemical states of the prepared catalysts. According to the fitting analysis of Ce 3d XPS (Figure 5c), the surface concentration of Ce^{3+} on Ce/Ti-M (25.4%) was much higher than that on Ce/Ti-L (17.5%), which should be due to the smaller CeO_2 particles on Ce/Ti-M, matching well with the expectation. However, Ce/Ti−H with highly dispersed Ce species showed a Ce^{3+} concentration (23.0%) that was lower than that of Ce/Ti-M, which meant that the formation of abundant Ce−O−Ti structures and the lack of crystalline CeO_2 were conducive to the generation of Ce^{3+} species. O 1s was also collected (Figure 5d). It was found that the concentration of surface-adsorbed oxygen species on CeO_2/TiO_2 catalysts decreased in the order of Ce/Ti-M > Ce/Ti−H > Ce/Ti-L. The higher concentration of surface Ce^{3+} and surface-adsorbed oxygen species was always related to better redox performance.[43,44] In addition, the results of Ti 2p XPS suggested that the electron donation from the TiO_2 support to small CeO_2 particles could be another reason for the generation of more Ce^{3+} on Ce/Ti-M (Figure S14).

To further investigate the effect of the redox capability on the activation of reactants, the reactivity of CeO_2/TiO_2 catalysts in NH_3 oxidation and NO oxidation reactions was evaluated. As shown in Figure 5e, Ce/Ti-M performed better than Ce/Ti−H and Ce/Ti-L in the NH_3 oxidation reaction, which meant that CeO_2 with moderate dispersion could effectively activate NH_3. It was also found that all CeO_2/TiO_2 catalysts showed comparable N_2 selectivity, although Ce/Ti-M performed the best among those CeO_2/TiO_2 catalysts (Figure S15). Moreover, as expected, Ce/Ti-M also showed the best NO oxidation activity among the three CeO_2/TiO_2 catalysts, indicating that NO could be better activated on Ce/Ti-M (Figure 5f). It could be inferred from the results of CO-TPR, XPS, NH_3 oxidation, and NO oxidation that TiO_2-supported CeO_2 with moderate dispersion (Ce/Ti-M) exhibited better low-temperature redox capability, which could better facilitate the activation of the reactants and further contribute to superior NH_3−SCR activity.

3.4. Reaction Mechanism. A systematic *in situ* DRIFTS study was designed to further elucidate the reaction mechanism on the CeO_2/TiO_2 catalysts. The reactivity of adsorbed NH_3 was first investigated by *in situ* DRIFTS of NO +O_2 reacting with preadsorbed NH_3. As shown in Figure 6a−c, NH_3 species adsorbed on Lewis acid sites (1173, 1227, and 1574/1594/1601 cm^{-1}, in red fonts) and Brønsted acid sites (1436 and 1695 cm^{-1}, in blue fonts) were observed on three CeO_2/TiO_2 catalysts when exposed to NH_3 flow.[42,45,46] The more intensive IR bands attributed to NH_3 adsorbed on Lewis acid sites (1173 and 1227 cm^{-1}) suggested that acid sites on the CeO_2/TiO_2 catalyst were dominant in the form of Lewis acid sites. According to the results of *in situ* DRIFTS of NH_3 adsorption on TiO_2 and CeO_2/TiO_2 catalysts (Figure S16), IR bands at ca. 1173 and 1574 cm^{-1} could be attributed to NH_3 adsorbed on Ce sites, while IR bands at ca. 1227 and 1601 cm^{-1} could be ascribed to NH_3 adsorbed on Ti sites. Upon the introduction of NO+O_2 to CeO_2/TiO_2 catalysts preadsorbed with NH_3, NH_3 species adsorbed on both Lewis acid sites and Bronsted acid sites were consumed gradually. Simultaneously, several bands attributed to nitrate species emerged (1365, 1535, 1552, and 1620 cm^{-1}).[39,47] The consumption of adsorbed NH_3 by NO+O_2 flow suggested that the NH_3−SCR reaction on CeO_2/TiO_2 catalysts could follow the Eley−Rideal (E−R) mechanism. To better compare the consumption rate of adsorbed NH_3, the normalized peak area of the band at 1173 cm^{-1} as a function of reaction time was plotted and is shown in Figure 6d. It was clearly demonstrated that the consumption rate of NH_3 on CeO_2/TiO_2 catalysts followed an order of Ce/Ti-M > Ce/Ti−H > Ce/Ti-L, and NH_3 adsorbed on Ce/Ti-M could be almost consumed in 10 min, further confirming that the efficient activation of NH_3 on Ce/Ti-M could be one of the main reasons for its better NH_3−SCR activity.

The reactivity of adsorbed nitrates on CeO_2/TiO_2 catalysts was also estimated by *in situ* DRIFTS of NH_3 reacting with preadsorbed NO_x (Figure 6e−g). Interestingly, the adsorption of NO_x on the CeO_2/TiO_2 catalysts was relatively weak. The bands at 1184, 1365, and 1552/1556 cm^{-1} could be assigned to bridging bidentate nitrates, nitro species, and monodentate species, respectively,[39,42,48] which were not consumed by introduced NH_3 throughout the experiment. In contrast, the band at *ca.* 1634 cm^{-1} related to adsorbed NO_2 species on Ce/Ti−H and Ce/Ti-M could be rapidly consumed by the NH_3 flow in the first 2 min,[49,50] indicating that the NH_3−SCR reaction on Ce/Ti−H and Ce/Ti-M could be efficiently proceeded by the Langmuir−Hinshelwood (L−H) mechanism. The generation of adsorbed NO_2 species should be due to the oxidation of NO on Ce/Ti-M and Ce/Ti−H with a better redox capability. In order to exclude the possibility of NO_2 reacting with NH_3 to form inert species, the IR spectra of NH_3 reacting with preadsorbed NO_x on Ce/Ti-M in the first 2 min were stacked and enlarged to better demonstrate the changes upon the introduction of NH_3 (Figure S17). It was clearly observed that no band attributed to adsorbed NO_x was enhanced or emerged (marked in black font), while the band attributed to adsorbed NO_2 decreased, suggesting that NO_2 was consumed by NH_3 through the L−H mechanism.

To simplify for better comprehension, the privilege reaction mechanism on CeO_2/TiO_2 catalysts is demonstrated in Figure 6g. For Ce/Ti-M, the NH_3−SCR reaction could be efficiently proceeded by both E−R and L−H mechanisms. Similarly, the NH_3−SCR reaction on Ce/Ti−H also followed E−R and L−

https://doi.org/10.1021/acsestengg.5c00151
ACS EST Engg. 2025, 5, 2060−2069

H mechanisms. However, due to the relatively inferior redox performance of Ce/Ti−H compared to that of Ce/Ti-M, Ce/Ti−H exhibited lower activity than Ce/Ti-M. For Ce/Ti-L, the NH_3−SCR reaction on it dominantly followed the E−R mechanism with low efficiency.

4. CONCLUSIONS

By utilizing the inherent properties of hydroxyl groups on the oxide support in promoting the dispersion of active sites, coupled with the distinct dispersion behaviors of various Ce precursors on supports, TiO_2-supported CeO_2 catalysts with gradient dispersions were successfully constructed. It was found that Ce/Ti-M with moderate dispersion of CeO_2 (slightly crystalline CeO_2) exhibited much better NH_3−SCR activity than Ce/Ti−H with highly dispersed CeO_2 (amorphous CeO_2) and Ce/Ti-L with highly crystalline CeO_2. Further mechanistic studies confirmed that the superior low-temperature redox capability of slightly crystalline CeO_2 on Ce/Ti-M mainly accounted for its satisfactory NH_3−SCR activity. The NH_3−SCR reaction on Ce/Ti-M efficiently proceeded by the E−R and L−H mechanisms. That is, the optimization of catalysts should extend beyond merely pursuing the high dispersion of active species, emphasizing instead the importance of customized design based on the unique characteristics of active species and their targeted reactions. This study provided valuable insights and fundamental knowledge for the rational design of high-performance catalysts, which held significant promise for advancing pollutant emission control technologies.

■ ASSOCIATED CONTENT

Supporting Information

The Supporting Information is available free of charge at https://pubs.acs.org/doi/10.1021/acsestengg.5c00151.

Details of catalyst characterizations and NH_3/NO oxidation activity evaluation, catalytic performance of recently reported CeO_2/TiO_2 catalysts, N_2-physisorption, NH_3-TPD, CO-TPR, H_2-TPR, HR-TEM images, XRD, NH_3-SCR activity, SO_2-TPD, DRIFTS study, ATR-FTIR, N_2 selectivity in NH_3 oxidation, and XPS (DOCX)

■ AUTHOR INFORMATION

Corresponding Authors

Qing Tong − *State Key Laboratory of Water Pollution Control and Green Resource Recycling, School of Environment, Jiangsu Key Laboratory of Vehicle Emissions Control, Centre for Shared Scientific Research Facilities, Key Laboratory of Mesoscopic Chemistry of MOE, School of Chemistry and Chemical Engineering, Nanjing University, Nanjing 210023, China*; Email: tongqing@nju.edu.cn

Wei Tan − *State Key Laboratory of Water Pollution Control and Green Resource Recycling, School of Environment, Jiangsu Key Laboratory of Vehicle Emissions Control, Centre for Shared Scientific Research Facilities, Key Laboratory of Mesoscopic Chemistry of MOE, School of Chemistry and Chemical Engineering, Nanjing University, Nanjing 210023, China*; orcid.org/0000-0002-1481-9346; Email: tanwei@nju.edu.cn

Lin Dong − *State Key Laboratory of Water Pollution Control and Green Resource Recycling, School of Environment, Jiangsu Key Laboratory of Vehicle Emissions Control, Centre for Shared Scientific Research Facilities, Key Laboratory of Mesoscopic Chemistry of MOE, School of Chemistry and Chemical Engineering, Nanjing University, Nanjing 210023, China*; orcid.org/0000-0002-8393-6669; Email: donglin@nju.edu.cn

Authors

Nan Jiang − *State Key Laboratory of Water Pollution Control and Green Resource Recycling, School of Environment, Jiangsu Key Laboratory of Vehicle Emissions Control, Centre for Shared Scientific Research Facilities, Key Laboratory of Mesoscopic Chemistry of MOE, School of Chemistry and Chemical Engineering, Nanjing University, Nanjing 210023, China*

Jiawei Yang − *State Key Laboratory of Water Pollution Control and Green Resource Recycling, School of Environment, Jiangsu Key Laboratory of Vehicle Emissions Control, Centre for Shared Scientific Research Facilities, Key Laboratory of Mesoscopic Chemistry of MOE, School of Chemistry and Chemical Engineering, Nanjing University, Nanjing 210023, China*

Yirui Yang − *State Key Laboratory of Water Pollution Control and Green Resource Recycling, School of Environment, Jiangsu Key Laboratory of Vehicle Emissions Control, Centre for Shared Scientific Research Facilities, Key Laboratory of Mesoscopic Chemistry of MOE, School of Chemistry and Chemical Engineering, Nanjing University, Nanjing 210023, China*

Wu Gao − *State Key Laboratory of Water Pollution Control and Green Resource Recycling, School of Environment, Jiangsu Key Laboratory of Vehicle Emissions Control, Centre for Shared Scientific Research Facilities, Key Laboratory of Mesoscopic Chemistry of MOE, School of Chemistry and Chemical Engineering, Nanjing University, Nanjing 210023, China*

Kaili Ma − *Analysis and Testing Center, Southeast University, Nanjing 211189, China*

Xiuwen Wang − *Center for Microscopy and Analysis, Nanjing University of Aeronautics and Astronautics, Nanjing 211106, China*

Qiuhui Qian − *National and Local Joint Engineering Laboratory of Municipal Sewage Resource Utilization Technology, School of Environmental Science and Engineering, Suzhou University of Science and Technology, Suzhou 215009, China*

Complete contact information is available at: https://pubs.acs.org/10.1021/acsestengg.5c00151

Author Contributions

⊥N.J. and J.Y. contributed equally to this work. CRediT: **Yirui Yang** writing - review & editing; **Wu Gao** formal analysis; **Kaili Ma** methodology.

Notes

The authors declare no competing financial interest.

■ ACKNOWLEDGMENTS

W.T. thanks the support from the National Natural Science Foundation of China (22306090), the Natural Science Foundation of Jiangsu Province (BK20230773), and the Young Elite Scientists Sponsorship Program by CAST (No. YESS20230298). L.D. thanks the support from the National Natural Science Foundation of China (22272077) and the

Natural Science Foundation of Jiangsu Province (BK20231513). Q.T. thanks the support from the National Natural Science Foundation of China (22476085). K.M. thanks the support from the National Natural Science Foundation of China (22402027).

REFERENCES

(1) Manisalidis, I.; Stavropoulou, E.; Stavropoulos, A.; Bezirtzoglou, E. Environmental and Health Impacts of Air Pollution: A Review. *Front. Public Health* **2020**, *8*, No. 14, DOI: 10.3389/fpubh.2020.00014.

(2) Chen, Y.; Liu, X.; Wang, P.; Mansoor, M.; Zhang, J.; Peng, D.; Han, L.; Zhang, D. Challenges and Perspectives of Environmental Catalysis for NO_x Reduction. *JACS Au* **2024**, *4* (8), 2767−2791.

(3) Damma, D.; Ettireddy, P. R.; Reddy, B. M.; Smirniotis, P. G. A Review of Low Temperature NH_3-SCR for Removal of NO_x. *Catalysts* **2019**, *9* (4), 349.

(4) Duan, C.; Zhang, Y.; Han, S.; Shan, Y.; Du, J.; Wang, M.; Shan, W. Recent advances in zeolites for the selective catalytic reduction of NO_x with NH_3. *Catal. Rev.* **2024**, 1−62.

(5) Han, L.; Cai, S.; Gao, M.; Hasegawa, J.-y.; Wang, P.; Zhang, J.; Shi, L.; Zhang, D. Selective Catalytic Reduction of NO_x with NH_3 by Using Novel Catalysts: State of the Art and Future Prospects. *Chem. Rev.* **2019**, *119* (19), 10916−10976.

(6) Chen, X.; Selloni, A. Introduction: Titanium Dioxide (TiO_2) Nanomaterials. *Chem. Rev.* **2014**, *114* (19), 9281−9282.

(7) Fröschl, T.; Hörmann, U.; Kubiak, P.; Kučerová, G.; Pfanzelt, M.; Weiss, C. K.; Behm, R. J.; Hüsing, N.; Kaiser, U.; Landfester, K.; Wohlfahrt-Mehrens, M. High surface area crystalline titanium dioxide: potential and limits in electrochemical energy storage and catalysis. *Chem. Soc. Rev.* **2012**, *41* (15), 5313−5360.

(8) Bagheri, S.; Muhd Julkapli, N.; Ben Abd Hamid, S. Titanium Dioxide as a Catalyst Support in Heterogeneous Catalysis. *Sci. World J.* **2014**, *2014* (1), No. 727496.

(9) Inomata, Y.; Hata, S.; Mino, M.; Kiyonaga, E.; Morita, K.; Hikino, K.; Yoshida, K.; Kubota, H.; Toyao, T.; Shimizu, K.-i.; et al. Bulk Vanadium Oxide versus Conventional V_2O_5/TiO_2: NH_3−SCR Catalysts Working at a Low Temperature Below 150 °C. *ACS Catal.* **2019**, *9* (10), 9327−9331.

(10) He, G.; Lian, Z.; Yu, Y.; Yang, Y.; Liu, K.; Shi, X.; Yan, Z.; Shan, W.; He, H. Polymeric vanadyl species determine the low-temperature activity of V-based catalysts for the SCR of NO_x with NH_3. *Sci. Adv.* **2018**, *4* (11), No. eaau4637.

(11) Lian, Z.; Wei, J.; Shan, W.; Yu, Y.; Radjenovic, P. M.; Zhang, H.; He, G.; Liu, F.; Li, J.-F.; Tian, Z.-Q.; He, H. Adsorption-Induced Active Vanadium Species Facilitate Excellent Performance in Low-Temperature Catalytic NO_x Abatement. *J. Am. Chem. Soc.* **2021**, *143* (27), 10454−10461.

(12) Lian, Z.; Liu, L.; Lin, C.; Shan, W.; He, H. Hydrothermal Aging Treatment Activates V_2O_5/TiO_2 Catalysts for NO_x Abatement. *Environ. Sci. Technol.* **2022**, *56* (13), 9744−9750.

(13) Zhao, W.; Zhang, K.; Wu, L.; Wang, Q.; Shang, D.; Zhong, Q. Ti^{3+} doped V_2O_5/TiO_2 catalyst for efficient selective catalytic reduction of NO_x with NH_3. *J. Colloid Interface Sci.* **2021**, *581*, 76−83.

(14) Li, Y.; Du, J.; Lin, C.; Lin, J.; Liu, J.; Cai, J.; Liu, C.; Lian, Z.; Shan, W. Improvement of Low-Temperature NH_3−SCR Activity over $CeVO_4$ Modified by Sm. *Ind. Eng. Chem. Res.* **2024**, *63* (42), 17824−17835.

(15) Tan, W.; Wang, J.; Li, L.; Liu, A.; Song, G.; Guo, K.; Luo, Y.; Liu, F.; Gao, F.; Dong, L. Gas phase sulfation of ceria-zirconia solid solutions for generating highly efficient and SO_2 resistant NH_3-SCR catalysts for NO removal. *J. Hazard. Mater.* **2020**, *388*, No. 121729.

(16) Shan, W.; Liu, F.; He, H.; Shi, X.; Zhang, C. An environmentally-benign CeO_2-TiO_2 catalyst for the selective catalytic reduction of NO_x with NH_3 in simulated diesel exhaust. *Catal. Today* **2012**, *184* (1), 160−165.

(17) Gong, Z.; Cao, J.; Hu, Y.; Yang, Y.; Ye, J.; Yao, X. Unraveling the contribution of acidic metal oxides modulating the CeO_2/TiO_2 catalyst acid sites for NH_3-SCR activity and SO_2 tolerance. *Sep. Purif. Technol.* **2025**, *362*, No. 131747.

(18) Cai, Y.; Ji, X.; Zhang, B.; Mu, Y.; Tong, Q.; Liu, A.; Tan, W.; Liu, F.; Dong, L. Research progress in ceria-based catalysts for the selective catalytic oxidation of NH_3. *Sci. Sin. Chim.* **2024**, *54* (3), 295−308.

(19) Tang, C.; Zhang, H.; Dong, L. Ceria-based catalysts for low-temperature selective catalytic reduction of NO with NH_3. *Catal. Sci. Technol.* **2016**, *6* (5), 1248−1264.

(20) Tan, C.; Han, Y.; Hu, Y.; Shen, K.; Ding, S.; Zhang, Y. Preparation and NH_3-SCR catalytic performance of $CeTiO_x$ catalysts with different pore structures. *J. Fuel Chem. Technol.* **2024**, *52* (1), 65−74.

(21) Zhang, L.; Li, L.; Cao, Y.; Yao, X.; Ge, C.; Gao, F.; Deng, Y.; Tang, C.; Dong, L. Getting insight into the influence of SO_2 on TiO_2/CeO_2 for the selective catalytic reduction of NO by NH_3. *Appl. Catal., B* **2015**, *165*, 589−598.

(22) Chen, L.; Li, J.; Ge, M.; Zhu, R. Enhanced activity of tungsten modified CeO_2/TiO_2 for selective catalytic reduction of NO_x with ammonia. *Catal. Today* **2010**, *153* (3), 77−83.

(23) Chen, X.; Cao, S.; Weng, X.; Wang, H.; Wu, Z. Effects of morphology and structure of titanate supports on the performance of ceria in selective catalytic reduction of NO. *Catal. Commun.* **2012**, *26*, 178−182.

(24) Ma, K.; Guo, K.; Li, L.; Zou, W.; Tang, C.; Dong, L. Cavity size dependent SO_2 resistance for NH_3-SCR of hollow structured CeO_2-TiO_2 catalysts. *Catal. Commun.* **2019**, *128*, No. 105719.

(25) Li, L.; Ge, C.; Ji, J.; Tan, W.; Wang, X.; Wei, X.; Guo, K.; Tang, C.; Dong, L. Effects of different methods of introducing Mo on denitration performance and anti-SO_2 poisoning performance of CeO_2. *Chin. J. Catal.* **2021**, *42* (9), 1488−1499.

(26) Xu, W.; Yu, Y.; Zhang, C.; He, H. Selective catalytic reduction of NO by NH_3 over a Ce/TiO_2 catalyst. *Catal. Commun.* **2008**, *9* (6), 1453−1457.

(27) Gao, X.; Jiang, Y.; Fu, Y.; Zhong, Y.; Luo, Z.; Cen, K. Preparation and characterization of CeO_2/TiO_2 catalysts for selective catalytic reduction of NO with NH_3. *Catal. Commun.* **2010**, *11* (5), 465−469.

(28) Shan, W.; Liu, F.; He, H.; Shi, X.; Zhang, C. The Remarkable Improvement of a Ce-Ti based Catalyst for NO_x Abatement, Prepared by a Homogeneous Precipitation Method. *ChemCatChem* **2011**, *3* (8), 1286−1289.

(29) Sun, J.; Ge, C.; Yao, X.; Zou, W.; Hong, X.; Tang, C.; Dong, L. Influence of different impregnation modes on the properties of CuO-CeO_2/γ-Al_2O_3 catalysts for NO reduction by CO. *Appl. Surf. Sci.* **2017**, *426*, 279−286.

(30) Tan, W.; Xie, S.; Zhang, X.; Ye, K.; Almousawi, M.; Kim, D.; Yu, H.; Cai, Y.; Xi, H.; Ma, L.; et al. Fine-Tuning of Pt Dispersion on Al_2O_3 and Understanding the Nature of Active Pt Sites for Efficient CO and NH_3 Oxidation Reactions. *ACS Appl. Mater. Interfaces* **2024**, *16* (1), 454−466.

(31) Crouthamel, C. E.; Martin, D. S. Solubility of the Rare Earth Oxalates and Complex Ion Formation in Oxalate Solution.2. Neodymium and Cerium(Iii). *J. Am. Chem. Soc.* **1951**, *73* (2), 569−573.

(32) Sugimoto, T.; Zhou, X.; Muramatsu, A. Synthesis of Uniform Anatase TiO_2 Nanoparticles by Gel−Sol Method: 1. Solution Chemistry of $Ti(OH)_n^{(4-n)+}$ Complexes. *J. Colloid Interface Sci.* **2002**, *252* (2), 339−346.

(33) Nguyen, D. M.; Ding, S.; Nghiem, T. T.; Nguyen, V. A.; Mejía, E. Visible Light-Driven Degradation of Trichloroethylene in Aqueous Phase with Vanadium-Doped TiO_2 Photocatalysts. *Sol. RRL* **2023**, *7* (6), No. 2200938.

(34) Al-Harbi, L. M.; Mohamed, W. S.; Ebnalwaled, A. A.; Said, A. H.; Ezzeldien, M. The effect of synthesis conditions on the photokilling activity of TiO_2 nanostructures. *Mater. Res. Express* **2023**, *10* (1), No. 015004.

https://doi.org/10.1021/acsestengg.5c00151
ACS EST Engg. 2025, 5, 2060−2069

(35) El-Deen, S. S.; Hashem, A. M.; Abdel Ghany, A. E.; Indris, S.; Ehrenberg, H.; Mauger, A.; Julien, C. M. Anatase TiO_2 nanoparticles for lithium-ion batteries. *Ionics* **2018**, *24* (10), 2925−2934.
(36) Tan, W.; Xie, S.; Cai, Y.; Yu, H.; Ye, K.; Wang, M.; Diao, W.; Ma, L.; Ehrlich, S. N.; Gao, F.; et al. Surface Lattice-Embedded Pt Single-Atom Catalyst on Ceria-Zirconia with Superior Catalytic Performance for Propane Oxidation. *Environ. Sci. Technol.* **2023**, *57* (33), 12501−12512.
(37) Zeng, Y.; Haw, K.-G.; Wang, Y.; Zhang, S.; Wang, Z.; Zhong, Q.; Kawi, S. Recent Progress of CeO_2-TiO_2 Based Catalysts for Selective Catalytic Reduction of NO_x by NH_3. *ChemCatChem* **2021**, *13* (2), 491−505.
(38) Tan, W.; Liu, A. N.; Xie, S. H.; Yan, Y.; Shaw, T. E.; Pu, Y.; Guo, K.; Li, L. L.; Yu, S. H.; Gao, F.; et al. Ce-Si Mixed Oxide: A High Sulfur Resistant Catalyst in the NH-SCR Reaction through the Mechanism-Enhanced Process. *Environ. Sci. Technol.* **2021**, *55* (6), 4017−4026.
(39) Tan, W.; Wang, C.; Yu, S.; Li, Y.; Xie, S.; Gao, F.; Dong, L.; Liu, F. Revealing the effect of paired redox-acid sites on metal oxide catalysts for efficient NO_x removal by NH_3-SCR. *J. Hazard. Mater.* **2021**, *416*, No. 125826.
(40) Wang, Z.; Jiao, M.; Chen, Z.; He, H.; Liu, L. Effects of montmorillonite and anatase TiO2 support on CeO2 catalysts during NH3-SCR reaction. *Microporous Mesoporous Mater.* **2021**, *320*, No. 111072.
(41) Hailstone, R. K.; DiFrancesco, A. G.; Leong, J. G.; Allston, T. D.; Reed, K. J. A Study of Lattice Expansion in CeO_2 Nanoparticles by Transmission Electron Microscopy. *J. Phys. Chem. C* **2009**, *113* (34), 15155−15159.
(42) Yao, X.; Zhao, R.; Chen, L.; Du, J.; Tao, C.; Yang, F.; Dong, L. Selective catalytic reduction of NO_x by NH_3 over CeO_2 supported on TiO_2: Comparison of anatase, brookite, and rutile. *Appl. Catal., B* **2017**, *208*, 82−93.
(43) Yang, J.; Zhou, H.; Luo, Y.; Cheng, Y. L.; Wang, S.; Yao, L.; Wan, Y. D.; Zhu, J. J. Insight into the promotion effects of Ce on the performances of V-Ti based catalyst for low-temperature NH3-SCR: In-situ spectroscopy studies. *Sep. Purif. Technol.* **2025**, *362*, No. 131714, DOI: 10.1016/j.seppur.2025.131714.
(44) Cao, J.; Gao, Y.; Yao, L.; Tian, S.; Yao, X.; Liu, W.; Liu, Q.; Chen, Y. Synergistic effect of Cerium and Niobium enhances the low-temperature NH_3-SCR activity of Fe-containing solid waste. *Sep. Purif. Technol.* **2025**, *354*, No. 129373.
(45) Peng, Y.; Li, K.; Li, J. Identification of the active sites on CeO_2-WO_3 catalysts for SCR of NO_x with NH_3: An in situ IR and Raman spectroscopy study. *Appl. Catal., B* **2013**, *140*−*141*, 483−492.
(46) Ma, Z.; Wu, X.; Si, Z.; Weng, D.; Ma, J.; Xu, T. Impacts of niobia loading on active sites and surface acidity in NbO_x/CeO_2-ZrO_2 NH_3-SCR catalysts. *Appl. Catal., B* **2015**, *179*, 380−394.
(47) Liu, J.; Li, X.; Zhao, Q.; Ke, J.; Xiao, H.; Lv, X.; Liu, S.; Tadé, M.; Wang, S. Mechanistic investigation of the enhanced NH_3-SCR on cobalt-decorated Ce-Ti mixed oxide: In situ FTIR analysis for structure-activity correlation. *Appl. Catal., B* **2017**, *200*, 297−308.
(48) Hadjiivanov, K. I. Identification of Neutral and Charged N_xO_y Surface Species by IR Spectroscopy. *Catal. Rev.* **2000**, *42* (1−2), 71−144.
(49) Sivachandiran, L.; Thevenet, F.; Rousseau, A.; Bianchi, D. NO_2 adsorption mechanism on TiO_2: An *in-situ* transmission infrared spectroscopy study. *Appl. Catal., B* **2016**, *198*, 411−419.
(50) Liu, C.; Malta, G.; Kubota, H.; Kon, K.; Toyao, T.; Maeno, Z.; Shimizu, K.-i. In Situ/Operando IR and Theoretical Studies on the Mechanism of NH_3−SCR of NO/NO_2 over H−CHA Zeolites. *J. Phys. Chem. C* **2021**, *125* (25), 13889−13899.

https://doi.org/10.1021/acsestengg.5c00151
ACS EST Engg. 2025, 5, 2060−2069